Geophysical Research Letters

RESEARCH LETTER
10.1029/2023GL105770

Key Points:

- We present a robust low-cost Autonomous Electrical Resistivity Tomography system for permafrost monitoring in polar and mountainous regions
- We introduce an open-source tool for processing and inverting large data sets, enabling quick and efficient extraction of key information
- Field experiments conducted in Antarctica show high-temporal-resolution imaging of ground freezing and thawing dynamics

Correspondence to:
M. Farzamian,
mohammad.farzamian@iniav.pt

Citation:
Farzamian, M., Blanchy, G., McLachlan, P., Vieira, G., Esteves, M., de Pablo, M. A., et al. (2024). Advancing permafrost monitoring with Autonomous Electrical Resistivity Tomography (A-ERT): Low-cost instrumentation and open-source data processing tool. *Geophysical Research Letters*, *51*, e2023GL105770. https://doi.org/10.1029/2023GL105770

Received 10 AUG 2023
Accepted 16 DEC 2023

Advancing Permafrost Monitoring With Autonomous Electrical Resistivity Tomography (A-ERT): Low-Cost Instrumentation and Open-Source Data Processing Tool

M. Farzamian[1,2], G. Blanchy[3], P. McLachlan[4], G. Vieira[2], M. Esteves[2], M. A. de Pablo[5], J. Triantafilis[6], E. Lippmann[7], and C. Hauck[8]

[1]Instituto Nacional de Investigação Agrária e Veterinária, Oeiras, Portugal, [2]Centre for Geographical Studies, Associate Laboratory TERRA, IGOT, Universidade de Lisboa, Lisbon, Portugal, [3]University of Liège, Liège, Belgium, [4]Aarhus University, Aarhus, Denmark, [5]Universidad de Alcalá, Alcalá de Henares, Spain, [6]Manaaki Whenua Landcare Research, Palmerston North, New Zealand, [7]Lippmann Geophysical Instruments (LGM), Schaufling, Germany, [8]Department of Geosciences, University of Fribourg, Fribourg, Switzerland

Abstract Permafrost is a widespread phenomenon in the cold regions of the globe and is under-represented in global monitoring networks. This study presents a novel low-cost, low-power, and robust Autonomous Electrical Resistivity Tomography (A-ERT) monitoring system and open-source processing tools for permafrost monitoring. The processing workflow incorporates diagnostic and filtering tools and utilizes open-source software, ResIPy, for data inversion. The workflow facilitates quick and efficient extraction of key information from large data sets. Field experiments conducted in Antarctica demonstrated the system's capability to operate in harsh and remote environments and provided high-temporal-resolution imaging of ground freezing and thawing dynamics. This data set and processing workflow allow for a detailed investigation of how meteorological conditions impact subsurface processes. The A-ERT setup can complement existing monitoring networks on permafrost and is suitable for continuous monitoring in polar and mountainous regions, contributing to cryosphere research and gaining deeper insights into permafrost and active layer dynamics.

Plain Language Summary Permafrost, frozen ground in cold regions, has significant impacts on the global environment. Monitoring of permafrost is crucial because it influences the global carbon cycle, hydrology, contaminant movement, and ecosystem stability. However, current monitoring systems have limitations, particularly in remote regions like Antarctica. To tackle this challenge, a new monitoring system, Autonomous Electrical Resistivity Tomography (A-ERT), was introduced. A-ERT is a geophysical technique that employs electrical signals to study ground freezes and thaws with high precision over time. Alongside this, open-source processing tools were developed to process obtained A-ERT data and efficiently extract essential information from large data sets. The developed A-ERT system is robust, low-cost, low-power, and designed to operate in harsh conditions. Tested in Antarctica, our findings show that A-ERT data combined with processing pipelines offers a valuable tool for examining freezing and thawing processes in extreme environments. The proposed setup can contribute to a network of autonomous permafrost monitoring systems, important for cryosphere research and advancing our understanding of climate change's impact on permafrost dynamics.

1. Introduction

Permafrost is a widespread phenomenon in the cold regions of the globe and is under-represented in global monitoring networks (Hock et al., 2019). Initiatives such as the Global Terrestrial Network for Permafrost (GTN-P) and the Circumpolar Active Layer Monitoring (CALM) networks were established to observe the response of the active layer and permafrost to climate change over long time scales (Brown et al., 2000). GTN-P primarily monitors borehole temperature, while CALM focuses on manual thaw depth measurements using mechanical probes (Ramos et al., 2017; Shiklomanov et al., 2008). Boreholes, while useful for monitoring the thermal state of permafrost, have limitations due to their high cost, localized nature, and limited numbers. Furthermore, drilling is invasive and impractical for extensive coverage, particularly in environmentally sensitive ecosystems like Antarctica. Mechanical probing is also not always feasible in areas with thick active layers with coarse, boulder-rich sediments. Additionally, given that mechanical probing is carried out usually once per year, it cannot provide a real-time monitoring of thaw depth progression. Moreover, it often fails to capture the maximum seasonal thaw depth, because accurately predicting when the maximum thaw depth will occur is challenging

and logistical constraints further hinder the ability to visit the site at the desired period for probing. Importantly, neither mechanical probing nor borehole temperatures provide information about the spatial and temporal variability of ground ice and unfrozen water content.

Electrical Resistivity Tomography (ERT) offers a solution to address some of the abovementioned problems. The method can detect the difference between unfrozen and frozen materials given the strong electrical resistivity contrasts, and allows monitoring of permafrost and active layer dynamics in two or three dimensions (Farzamian et al., 2020). Previous applications of ERT in cold environments have included investigating the freeze and thaw of the active layer in the European Alps (Hilbich et al., 2008; Mewes et al., 2017), North America (Uhlemann et al., 2021), Greenland (Doetsch et al., 2015; Tomaškovičová & Ingeman-Nielsen, 2023) and Antarctica (Hauck et al., 2007), estimating unfrozen water content distribution through time (Hauck, 2002; Oldenborger & LeBlanc, 2018), and assessing ground ice degradation (Hilbich et al., 2022).

Despite the potential for ERT monitoring in a climate change context (Mollaret et al., 2019), only a few operational long-term ERT monitoring sites exist in permafrost regions (Hilbich et al., 2008; Scandroglio et al., 2021; Supper et al., 2014). Furthermore, in all cases, these systems are operated manually and therefore need to be visited regularly, which makes it logistically complex and expensive, particularly for remote areas. Autonomous Electrical Resistivity Tomography (A-ERT) systems are a logical, and necessary extension of manually repeated measurements, as they enable the continuous acquisition of temporally dense ERT data sets. However, to date, only very few systems for permafrost exist (Farzamian et al., 2020; Hilbich et al., 2011; Keuschnig et al., 2017; Uhlemann et al., 2021). To instrument a greater number of stations, there is a need for systems that are inexpensive, robust in harsh climates, and that require minimal power to operate.

This work reports on how a low-cost, robust, low-power setup coupled with efficient processing tools provides valuable insight into subsurface dynamics in polar regions. The first prototype of the A-ERT system (prototype I) was developed in 2009 and was installed and tested on Deception Island, Antarctica, in 2010 (Farzamian et al., 2020). Several improvements were made to this prototype, and a new A-ERT system (prototype II) was manufactured and installed on Livingston Island, Antarctica, in 2020. This manuscript has three primary objectives: (a) to describe the details of this new and successfully tested A-ERT system, which was specifically adapted to deployments in harsh and remote terrains, where maintenance and repair is not possible regularly (b) to present a semi-automated processing workflow to filter and invert large number of A-ERT data sets, and (c) to highlight active layer dynamics and their typical electrical resistivity patterns in a case study. The manuscript also provides access to the data, figures, and Python-based open-source codes used for data processing in Jupyter Notebooks (see Farzamian et al., 2023).

2. Materials and Methods

2.1. Study Area and Monitoring Setup

Figure 1a shows the location of the Reina Sofia Peak (RSP) site in Hurd Peninsula (Livingston Island, Antarctica) where we installed the prototype II A-ERT system in 2020. Permafrost temperature monitoring at RSP began in 2000 in two shallow boreholes, including ground surface and air temperatures. Since 2007, snow cover thickness has been estimated using iButton temperature loggers at various heights above the ground on a wooden mast (Ramos & Vieira, 2009). The approach proposed by Lewkowicz (2008) was used to identify covered or free sensors based on daily temperature variability. RSP has an elevation of 275 m above sea level and the summit shows a flat, wind-exposed surface with approximately 100 × 50 m. The bedrock is the Myers Bluff Formation, a combination of fine sandstones and shales that in the surface have been frost shattered forming a diamicton of loose material approximately 1 m thick (Pimpirev et al., 2006). The thickness of this layer corresponds approximately to the active layer thickness, as determined by temperature data from a 25 m borehole with a permafrost temperature at the zero annual amplitude depth of about −1.8°C (Ramos et al., 2020). The climate is cold and maritime, with annual temperatures ranging from −1.9 to −1.2°C at sea level (Ramos, Vieira, Gruber, et al., 2008) and −4.2°C at the RSP (Ramos, Vieira, Blanco, et al., 2008).

2.2. Instrumentation

ERT methods involve injecting electrical current using two current electrodes (A and B) and measuring the resultant voltage between another two electrodes (M and N). Different portions of the subsurface can be interrogated

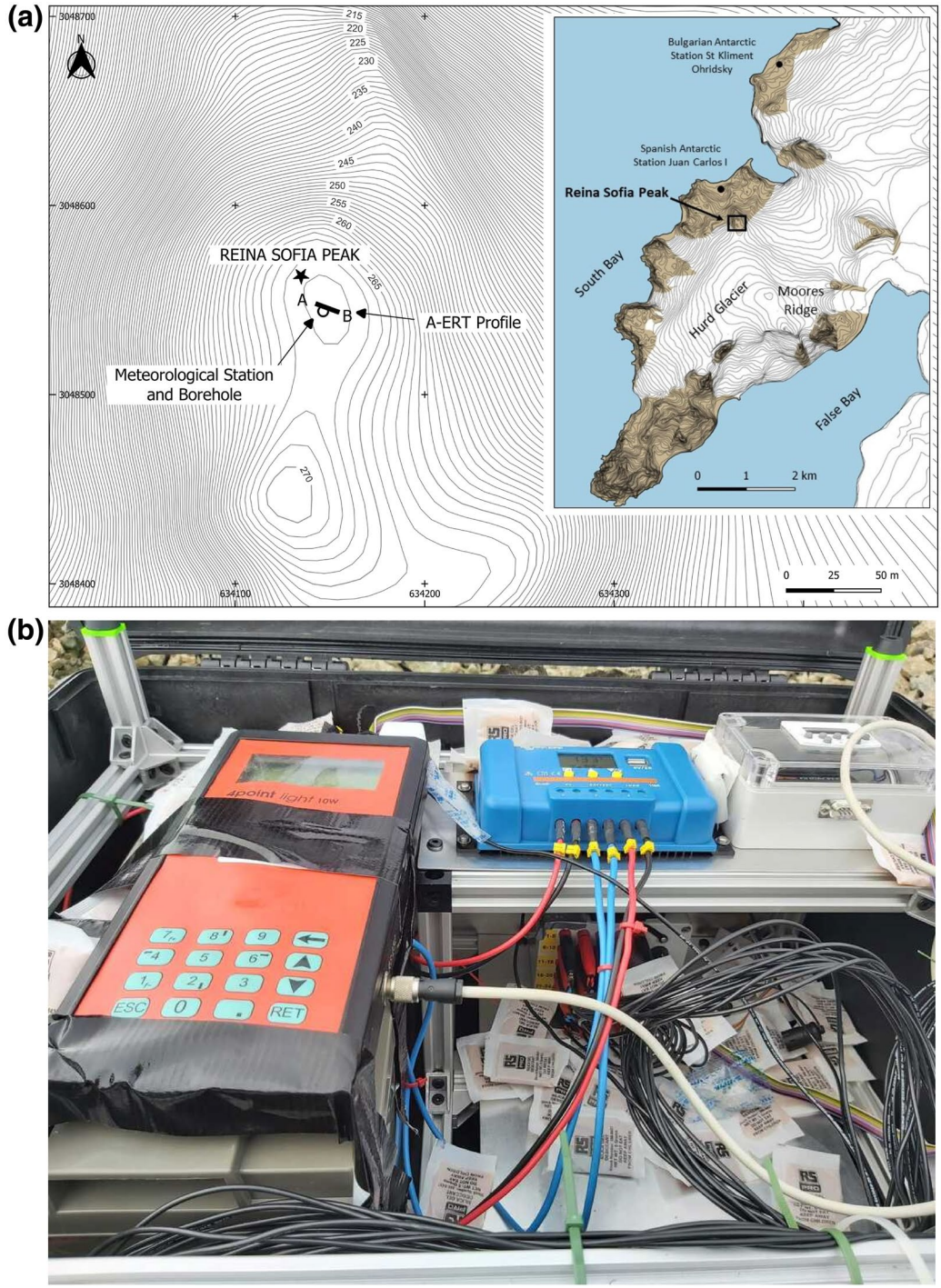

Figure 1. (a) Location of the Reina Sofia Peak and current monitoring setups in the site. (b) A-ERT equipment at Reina Sofia Peak.

by utilizing different combinations of electrodes along a transect (for an introduction of ERT method, see Binley, 2015). The electrodes, instrument, and power source are connected by cables. The A-ERT system components presented here include water-resistant cases, temperature-rated cables, and ruggedized mil-rated connectors so that the system can operate in harsh environments such as Antarctica. Autonomous operation is crucial in polar regions as frequent visits to polar locations can be prohibitively expensive, making it impractical to rely on manual monitoring. Although solar power can be used for most of the year, there are 3–4 months with very

Table 1
Components of the A-ERT System Installed in Reina Sofia Peak, Livingston Island

Component	Cost [EUR]	Manufacturer
4-point light 10 W	3,700	Lippmann
Switch boxes 26	2,400	Lippmann
Battery (AGM deep cycle 12V/110Ah)	190	Victron
Solar panel 30W/12V (x2)	50	Victron
Solar charge controller PWM 12/24V - 10A	25	Victron
Cables	170	AlphaWire
Customized weather resistant case (IP67 and MIL810F rated)	390	Explorer Cases
MIL Spec connectors	380	Amphenol
Timer	30	
Electrodes	150	
Aluminum supporting structure (interior of the case)	210	RatRig
Consumables (e.g., gaskets, banana plugs, terminals, screws)	140	

Note. The costs reflect the price at the time of purchase in 2019.

reduced insolation during the polar winter. Consequently, low-power consumption is also required since the regular replacement of batteries is not feasible.

The A-ERT system developed and adapted to the specific needs of remote, polar operation, has an approximate cost of 8,000 € in 2019 for a multi-electrode setup comprising 26 electrodes. It incorporates various components, as specified in Table 1. This low-cost A-ERT system will enable a more extensive deployment of A-ERT systems in permafrost regions on a global scale. The core of the system consists of a 4-point light 10 W resistivity meter (Figure 1b) that is lightweight (less than 1 kg), compact, low-cost, and low-power, making it easy to ship and carry to distant locations and operate autonomously. Its output current range is 1 μA–100 mA, with the minimum transmitter current of 1 μA being about one order of magnitude lower than the current resolution of conventional resistivity meters. This feature makes it suitable for monitoring the extremely high resistivities in permafrost areas without overloading the receiver circuit.

Measuring high resistivities at low currents is another challenge in permafrost areas and can result in low-quality data due to noise and measurement inaccuracies (Supper et al., 2014). The low-power switch boxes address these issues using an integrated buffer amplifier with an extremely high DC input impedance (>>1 GOhm), which minimizes errors with high contact resistance electrodes. The amplifiers' low output impedance reduces crosstalk between transmitter and receiver lines. An additional ground electrode is necessary to define the system's internal reference potential because the amplifiers have virtually infinite DC input impedance.

Water-resistant cases encased all electronic components (Figure 1b), and rugged mil-rated connectors, detailed in Table 1, were used to ensure no water entered the box. The 4-point light 10W device was standalone for autonomous monitoring, but it was programmed at the start of the survey using the GeoTest software (https://www.geophysik-dr-rauen.de/).

The Wenner electrode configuration was used with 26 electrodes spaced at 0.5 m intervals. Measurements were taken every 6 hr with a minimum of 5 and a maximum of 9 stacks per quadrupole and a target standard deviation of 2%. Data was stored in the resistivity meter's internal memory. This setup yields 100 individual data points for each monitoring data set at eight pseudo-depth levels.

Cold-rated 110 Ah deep cycle gel batteries were used for the 3–4 months of operation when solar power was unavailable. A timer was integrated into prototype II to activate and deactivate the resistivity meter before and after each data acquisition. Although the power consumption of the resistivity meter in standby mode is very low, approximately 250 mW, monitoring battery voltage of prototype I and incoming radiation during 3 years of observation at Deception Island revealed that this accounted for the highest portion of the system's power demand at this site. Therefore, integrating a timer into prototype II was necessary to reduce the overall energy consumption

significantly. The Jupyter Notebook (see Farzamian et al., 2023) presents the details of this evaluation and the improvements in power efficiency resulting from the timer integration, along with corresponding data and plots.

2.3. Data Processing and Inversion

For interpretation, ERT data needs to be modeled using geophysical inversion (see Binley, 2015). In this work, the ERT data are processed before being inverted using ResIPy (Blanchy et al., 2020). Processing predominantly comprises robust filtering methods to cull erroneous data. Filtering is especially necessary for time-lapse data sets; errors (e.g., associated with high contact resistances) can propagate through sequential resistivity models and result in erroneous interpretations. Ordinarily, data quality can be assessed with reciprocal measurements (Tso et al., 2017); however, reciprocal measurements were not collected to reduce power consumption. Consequently, additional metrics for assessing data quality were needed.

To identify system parameters indicative of poor data quality, we analyzed the time series of apparent resistivities, transmitter voltage (Vtx), current injection, contact resistances, the voltage at MN (U0), and stacking errors. Through this approach, we identified necessary filtering criteria; these criteria can be summarized as follows:

1. MN voltage measurements below or equal to 1 mV were removed.
2. Data with a stacking MN voltage error above 0.5% were removed.
3. A 6-hourly data set was kept if more than 80% of the measurements met the quality criteria above.

The third step was to ensure comparable sensitivity patterns were present in each 6-hourly data set. For instance, if two sequential data sets contain data with a substantially different number of measurements after filtering, inversion artifacts are likely to arise.

After filtering, the ERT data sets were inverted using ResIPy (Blanchy et al., 2020), which utilizes the R2 inversion code (Binley, 2015). There are several approaches for inverting time-lapse ERT data. The simplest is to invert data sets independently, which has been widely used (e.g., McLachlan et al., 2020). Although simple, such approaches are robust against error propagation in sequential models. However, the non-unique nature of ERT inversions means that this approach can result in abrupt temporal changes in modeled resistivity, especially if data quality is poor. Alternatively, difference inversions (LaBrecque & Yang, 2001) can be implemented, whereby data differences are inverted to minimize abrupt changes between sequential data sets. However, as Lesparre et al. (2017) noted, care needs to be given when assessing measurement error. In our study, difference inversions led to artifacts close to the electrodes, possibly due to significant changes in contact resistances associated with freezing and thawing events. Therefore, a background-constrained inversion approach was used whereby the inversion process is constrained to a starting model, in this case, the first data set. This approach ensures the resistivity distribution stays smooth through time and enables parallel processing of several surveys.

3. Results and Discussion

3.1. Apparent-Resistivity Data

For visualization across the 2 years, the measured apparent resistivities were averaged for each pseudo-depth level (Figure 2a). The pseudo-depth levels were calculated based on the distance between current electrodes. Figures 2b–2e presents the measured parameters for 100 quadrupoles, sorted by pseudo-depth level, as a diagnostic tool for identifying bad data. In these plots, quadrupoles are numbered from 1 to 100 starting with the shallowest pseudo-depth level and advancing to progressively deeper pseudo-depth levels. Sorting the data by pseudo-depth levels will enable determining whether poor data quality is linked to pseudo-depth levels.

One error source in our study was caused by overloaded voltages from the MN electrodes. For instance, given the 700 mV peak-to-peak upper limit for the voltage measurements, the maximum apparent resistivity that can be measured with the minimum current of 1 μA in a Wenner configuration and pseudo-depth level of 1.5 m is about 1 MOhm.m. The occurrence of this error can be identified by all measured parameters except for the current, being zero. In this case, the system reduces the current to its lowest possible value, 1 μA, while the voltage across the MN electrodes (U0) remains above the instrument's measurement range. This group of data was removed based on the first filtering criterion. Given the maximum apparent resistivity limit increases as the electrode spacing increases for larger pseudo-depth levels, this resolution error mostly affects measurements at pseudo-depth level of 1.5 m (see Figure 3g). To tackle this issue, a larger input voltage range will be implemented in the future setups.

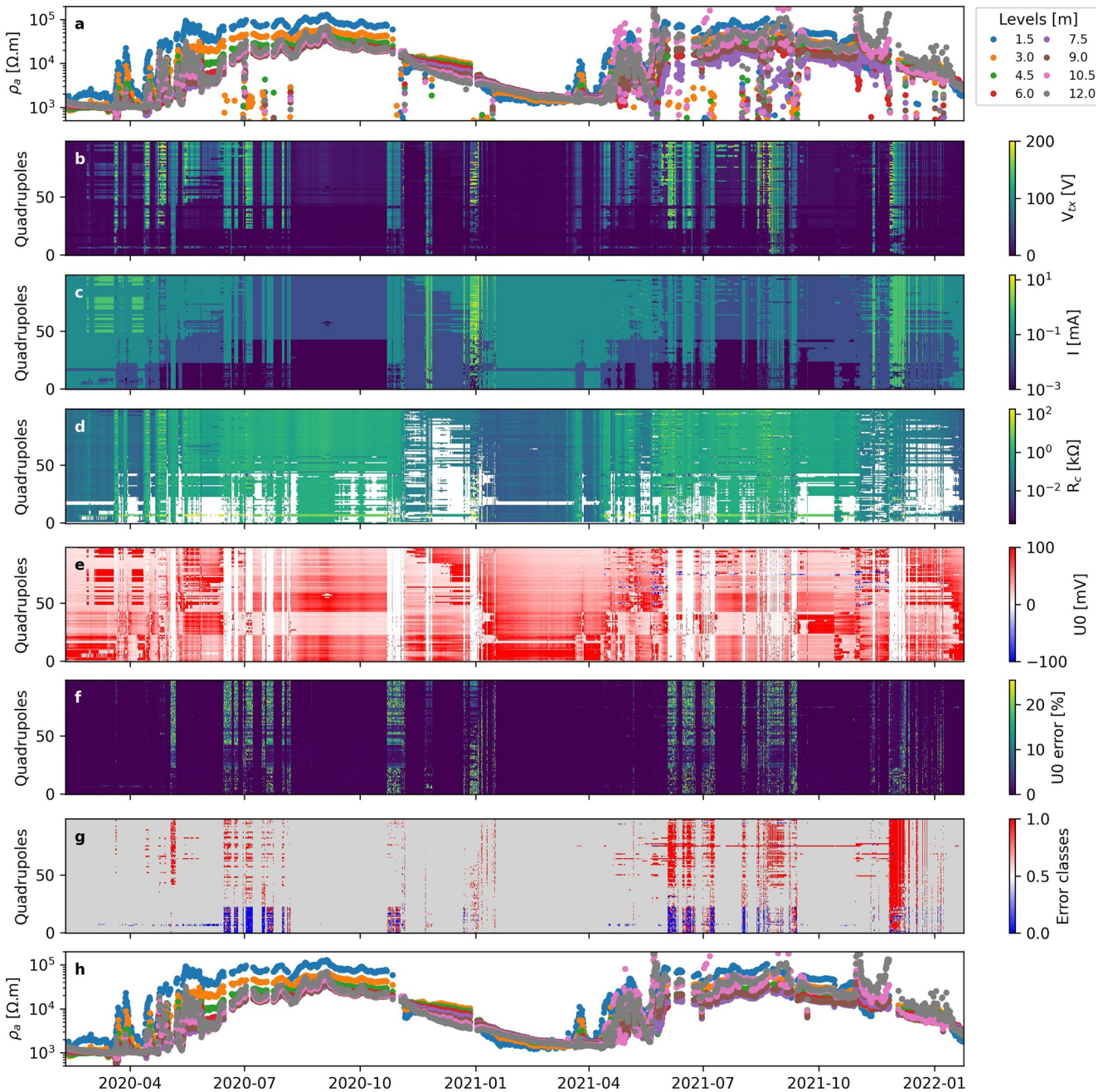

Figure 2. Raw (a–f) and filtered data (h) for the RSP site. (a) Apparent resistivity data. (b) Transmitter voltage. (c) Injected current. (d) Contact resistance. (e) The measured voltage at the MN electrodes. (f) Stacking error. (g) Shows the different error classes detected (0 = MN overload and 1 = saturation of amplifiers). (h) Filtered apparent resistivities data.

Figure 2 also illustrates another filtering criterion, which is based on the MN voltage (U0) being close to 0 mV (<1 mV). This effect occurs when the electronic amplifiers of the MN electrodes become saturated, leading to a measured U0 value close to 0 mV (Figure 2e). Under these conditions, the applied voltage at the transmitter typically exceeds 20 V (Figure 2b), resulting in a relatively high stacking error (Figure 2f). A plausible explanation for this phenomenon could be the poor contact of ground electrodes in a very resistive environment. When the ground electrode is weakly connected or disconnected, the input amplifier drifts into DC overload. It may produce spurious data, preventing the device from decreasing its current to a low enough value for voltage measurement at the MN electrodes. In these cases, we have noticed that the voltage at the transmitter is relatively

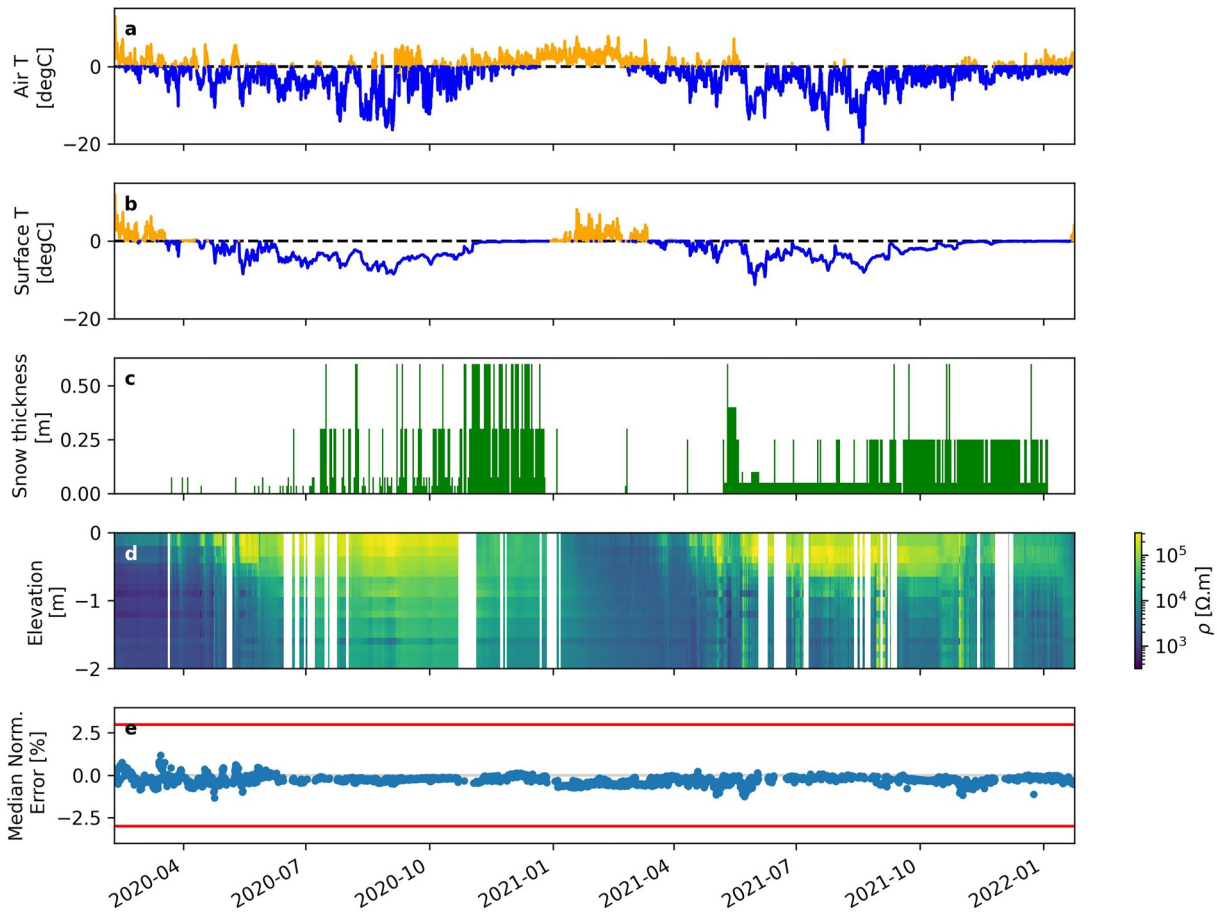

Figure 3. (a) Air and (b) soil temperature evolution along with (c) snow cover thickness for Livingston. (d) Inverted ERT profiles are taken in the middle of the transect. (e) Median normalized error after inversion in percentage (see Binley et al., 1995 for more information).

higher (typically above 20 V), and the injected current is also larger than the typical value during winter. The contact resistances are very high during these periods (>100 kOhm). Still, they remain consistent regardless of whether the AB voltage is above or below 20 V. This suggests that the high contact resistances are less likely to cause erroneous values. An additional factor contributing to these bad measurements could be the capacitive crosstalk between the current and ground cables, which could be significant when contact resistances are exceptionally high. This crosstalk can trigger a substantial voltage drop at the ground electrode, causing the electronic amplifiers of the MN electrodes to saturate. To tackle this issue, the ground electrode/cable will be excluded in the future setups, and a 100 MOhm input resistor was introduced to switch boxes. When used as potential electrodes, this resistor loads the electrodes, making the ground electrode unnecessary while having minimal impact on the measured values.

As mentioned in this section, only data sets containing more than 80% reliable data were retained. This approach removed almost 21% of data sets, primarily from winter. Figure 3h shows the filtered data used for the inversion. The apparent resistivity data collected at different pseudo-depth levels provide valuable insights into the freezing and thawing dynamics of the active layer. For example, the onset of seasonal freezing is indicated by a sharp rise in resistivity in May in both years, while the delayed response of deeper levels suggests the progression of the freezing front. The seasonal thawing phase is associated with a steady decrease in resistivity in November/December in 2021 and 2022.

Our investigation indicates that the diagnostic plots and filtering scheme proposed in this study can effectively identify and eliminate erroneous measurements, resulting in data sets of high quality suitable for the inversion process. In the event that the proposed criteria do not fully remove all bad measurements, additional processing criteria, suggested by Herring et al. (2023), can be implemented based on the data quality.

3.2. Inversion Results and Temporal Resistivity Variability

Figure 3 shows the evolution of the inverted resistivity at RSP alongside snow thickness, air temperature, and ground surface temperature (GST). The inversion converged well and the majority median normalized error after inversion (Binley et al., 1995) falls within the ±3% (Figure 3e). Each survey is represented by a vertical inverted resistivity profile taken from the middle of the ERT profile. A clear negative correlation can be observed between resistivity and GST in both active layer and permafrost zones. The bedrock at the site is also composed of layers of quartzite and claystones, which are fractured and not massive, resulting in a structure prone to water content fluctuations, which will result in variability of resistivity values with temperature. The impact of snow cover on GST and resistivities is clearly seen, for example, in November/December 2020 and 2021, when the zero-curtain effect (temperatures remain at the melting point during phase change) in the GST reveals the effect of snowmelt. Simultaneously, while snow insulates the ground from the positive air temperatures, delaying thawing, the snow meltwater may infiltrate the ground surface, transferring heat and reducing resistivities (Hilbich et al., 2011).

Sudden freezing events can be observed in May 2020 and 2021, with sharp resistivity increases in the near-surface. This occurs due to the absence of snow cover at the beginning of the freezing season, the cold air temperature, or high radiation losses which promote fast freezing, resulting in sharp resistivity increases. Interestingly, the drop in surface temperature in May 2021 is followed by a few weeks of positive air temperature and snowfall. This contributed to the decrease in resistivity observed at the beginning of June 2021, before a longer period of freezing. While the snow cover prevented phase change, snow melting provided water to the subsurface and decreased the resistivity during the event.

Several brief, shallow freezing events associated with abrupt resistivity increase can also be identified during March 2020 and 2021 before seasonal freezing in May. The short-lived meteorological events associated with brief subsurface freezing or thawing identified in the RSP data set are similar to those reported by Farzamian et al. (2020) in Deception Island. This suggests that such events are probably common in Maritime Antarctica. Despite the occurrence of phase-change processes and their potential impact on upper soil layers, permafrost studies often overlook these events. A-ERT method shows significant potential for evaluating their occurrence and impact in the region and globally, emphasizing the importance of A-ERT monitoring in permafrost regions.

4. Conclusion and Outlook

Low-cost, robust, and low-powered monitoring resistivity systems, such as the A-ERT, offer a unique means to investigate detailed freezing and thawing processes in remote permafrost regions. Here, we introduced an adapted A-ERT monitoring system to the harsh and remote conditions of Antarctica. Additionally, we highlighted sources of errors linked to such extreme environments through the analysis of data from a field example on Livingston Island. The experiences from the Livingston Island system resulted in a renewed system as part of the PERM^{2}ERT project (www.unifr.ch/geo/cryosphere/en/projects/permafrost-monitoring-and-dynamics/perm2ert.html), with further developments that will include two-way satellite communication, making it possible to easily retrieve data and remotely change the measurement frequency. This development will enable continuous and automated data processing throughout the year, real-time data visualization, optimizing the measurement frequency for the desired target process/event, adjusting power consumption to avoid data gaps, and evaluating in advance whether a site visit and system maintenance are required.

Data processing of resistivity time series in such harsh environments must be carefully executed before any interpretation. The processing pipeline developed in this work, supported by the companion Jupyter Notebook, forms the basis of semi-autonomous high-throughput processing for dense temporal data sets provided by A-ERT systems. Inverted resistivity profiles clearly showed relationships with GST and snow cover thickness for 2 years. Future improvements could involve using a time-lapse error model (Lesparre et al., 2017) and collecting reciprocal measurements to enhance filtering and establish an error model. While collecting additional reciprocal quadrupoles incurs additional costs in power consumption, the current monitoring of power demand and voltage in the A-ERT prototype II indicates that incorporating these measurements in future iterations is feasible.

The A-ERT prototypes combined with processing pipelines can be valuable tools in integrating resistivity measurements into other data collection in polar and extreme conditions, such as the GTN-P network of borehole temperatures in permafrost (Biskaborn et al., 2015). A-ERT data, along with water content and temperature monitoring systems, would allow integrated process studies within a coupled approach to be conducted in extreme and

polar environments (as shown for the European Alps, e.g., Hilbich et al., 2011). So far, only manually conducted, yearly repeated ERT measurements at a few reference stations exist to analyze permafrost degradation phenomena in larger detail than borehole temperatures can provide (Etzelmüller et al., 2020; Mollaret et al., 2019). A network of fully autonomous and continuous A-ERT measurements would largely contribute to studying the impact of fast-changing meteorological conditions on permafrost and the frequent freeze-thaw processes on soil behavior that cannot be determined solely from borehole information.

Data Availability Statement

The Jupyter Notebooks for data processing and inversion, along with the A-ERT, climate, and ground temperature data, are available in Farzamian et al. (2023).

Acknowledgments
The research received logistical support from the Portuguese Polar Program (PROPOLAR-FCT) within the ANTERMON and PERMANTAR projects and the Spanish Polar Program within the PERMATHERMAL project. The University of Fribourg and the Centre of Geographical Studies, IGOT - University of Lisbon provided financial support to develop the A-ERT system. This work received funding from the Swiss Polar Institute (grant number TEG-2021-003) and the Fundação para a Ciência e a Tecnologia under the project THAWIMPACT (2022.06628.PTDC). We thank the Spanish Antarctic Station "Juan Carlos I," and the BIO "Hespérides" personnel for logistical support and the continued support of the Spanish Polar Committee for the research on Livingston Island.

References

Binley, A. (2015). Tools and techniques: Electrical methods. In G. Schubert (Ed.), *Treatise on geophysics* (2nd ed., pp. 233–259). Elsevier. https://doi.org/10.1016/B978-0-444-53802-4.00192-5

Binley, A., Ramirez, A., & Daily, W. (1995). Regularised image reconstruction of noisy electrical resistance tomography data. In *Proceedings of the 4th workshop of the European concerted action on process tomography* (pp. 6–8).

Biskaborn, B. K., Lanckman, J. P., Lantuit, H., Elger, K., Streletskiy, D. A., Cable, W. L., & Romanovsky, V. E. (2015). The new database of the global terrestrial network for permafrost (GTN-P). *Earth System Science Data*, *7*(2), 245–259. https://doi.org/10.5194/essd-7-245-2015

Blanchy, G., Saneiyan, S., Boyd, J., McLachlan, P., & Binley, A. (2020). ResIPy, an intuitive open source software for complex geoelectrical inversion/modeling. *Computers & Geosciences*, *137*, 104423. https://doi.org/10.1016/j.cageo.2020.104423

Brown, J., Nelson, F. E., & Hinkel, K. M. (2000). The circumpolar active layer monitoring (CALM) program research designs and initial results. *Polar Geography*, *3*, 165–258.

Doetsch, J., Ingeman-Nielsen, T., Christiansen, A. V., Fiandaca, G., Auken, E., & Elberling, B. (2015). Direct current (DC) resistivity and induced polarization (IP) monitoring of active layer dynamics at high temporal resolution. *Cold Regions Science and Technology*, *119*, 16–28. https://doi.org/10.1016/j.coldregions.2015.07.002

Etzelmüller, B., Guglielmin, M., Hauck, C., Hilbich, C., Hoelzle, M., Isaksen, K., et al. (2020). Twenty years of European mountain permafrost dynamics-the PACE legacy. *Environmental Research Letters*, *15*(10), 104070. https://doi.org/10.1088/1748-9326/abae9d

Farzamian, M., Blanchy, G., McLachlan, P., Vieira, G., Esteves, M., de Pablo, M. A., et al. (2023). Advancing permafrost monitoring with autonomous electrical resistivity tomography (A-ERT): Low-cost instrumentation and open-source data processing tool (v1.0.0) [Software]. Zenodo. https://doi.org/10.5281/zenodo.10183126

Farzamian, M., Vieira, G., Monteiro Santos, F. A., Yaghoobi Tabar, B., Hauck, C., Catarina Paz, M., et al. (2020). Detailed detection of active layer freeze-thaw dynamics using quasi-continuous electrical resistivity tomography (Deception Island, Antarctica). *The Cryosphere*, *14*(3), 1105–1120. https://doi.org/10.5194/tc-14-1105-2020

Hauck, C. (2002). Frozen ground monitoring using DC resistivity tomography. *Geophysical Research Letters*, *29*(21), 2016. https://doi.org/10.1029/2002GL014995

Hauck, C., Vieira, G., Gruber, S., Blanco, J. J., & Ramos, M. (2007). Geophysical identification of permafrost in Livingston Island, maritime Antarctica. *Geophysical Research Letters*, *112*(F2), F02S19. https://doi.org/10.1029/2006JF000544

Herring, T., Lewkowicz, A. G., Hauck, C., Hilbich, C., Mollaret, C., Oldenborger, G. A., et al. (2023). Best practices for using electrical resistivity tomography to investigate permafrost. *Permafrost and Periglacial Processes*, *34*(4), 494–512. https://doi.org/10.1002/ppp.2207

Hilbich, C., Fuss, C., & Hauck, C. (2011). Automated time-lapse ERT for improved process analysis and monitoring of frozen ground. *Permafrost and Periglacial Processes*, *22*(4), 306–319. https://doi.org/10.1002/ppp.732

Hilbich, C., Hauck, C., Hoelzle, M., Scherler, M., Schudel, L., Völksch, I., et al. (2008). Monitoring mountain permafrost evolution using electrical resistivity tomography: A 7-year study of seasonal, annual, and long-term variations at Schilthorn, Swiss Alps. *Journal of Geophysical Research*, *113*(1), 1–12. https://doi.org/10.1029/2007JF000799

Hilbich, C., Hauck, C., Mollaret, C., Wainstein, P., & Arenson, L. U. (2022). Towards accurate quantification of ice content in permafrost of the Central Andes—Part 1: Geophysics-based estimates from three different regions. *The Cryosphere*, *16*(5), 1845–1872. https://doi.org/10.5194/tc-16-1845-2022

Hock, R., Rasul, G., Adler, C., Cáceres, B., Gruber, S., Hirabayashi, Y., et al. (2019). High mountain areas. In H. O. Pörtner, D. C. Roberts, V. Masson-Delmotte, P. Zhai, M. Tignor, E. Poloczanska, et al. (Eds.), *The ocean and cryosphere in a changing climate*, *Intergovernmental panel on climate change* (pp. 2-1–2-90). Retrieved from https://report.ipcc.ch/srocc/pdf/SROCC_FinalDraft_FullReport.pdf

Keuschnig, M., Krautblatter, M., Hartmeyer, I., Fuss, C., & Schrott, L. (2017). Automated electrical resistivity tomography testing for early warning in unstable permafrost rock walls around Alpine infrastructure. *Permafrost and Periglacial Processes*, *28*(1), 158–171. https://doi.org/10.1002/ppp.1916

LaBrecque, D. J., & Yang, X. (2001). Difference inversion of ERT data: A fast inversion method for 3-D in situ monitoring. *Journal of Environmental & Engineering Geophysics*, *6*(2), 83–89. https://doi.org/10.4133/jeeg6.2.83

Lesparre, N., Nguyen, F., Kemna, A., Robert, T., Hermans, T., Daoudi, M., & Flores-Orozco, A. (2017). A new approach for time-lapse data weighting in ERT. *Geophysics*, 1–35. https://doi.org/10.1190/geo2017-0024.1

Lewkowicz, A. G. (2008). Evaluation of miniature temperature-loggers to monitor snowpack evolution at mountain permafrost sites, northwestern Canada. *Permafrost Periglac*, *19*(3), 323–331. https://doi.org/10.1002/ppp.625

McLachlan, P., Chambers, J., Uhlemann, S., & Binley, A. (2020). Electrical resistivity and induced polarization imaging of riverbed sediments: Observations from laboratory, field and synthetic experiments. *Journal of Applied Geophysics*, *183*, 104173. https://doi.org/10.1016/j.jappgeo.2020.104173

Mewes, B., Hilbich, C., Delaloye, R., & Hauck, C. (2017). Resolution capacity of geophysical monitoring regarding permafrost degradation induced by hydrological processes. *The Cryosphere*, *11*(6), 2957–2974. https://doi.org/10.5194/tc-11-2957-2017

Mollaret, C., Hilbich, C., Pellet, C., Flores-Orozco, A., Delaloye, R., & Hauck, C. (2019). Mountain permafrost degradation documented through a network of permanent electrical resistivity tomography sites. *The Cryosphere*, *13*(10), 2557–2578. https://doi.org/10.5194/tc-13-2557-2019

Oldenborger, G. A., & LeBlanc, A. M. (2018). Monitoring changes in unfrozen water content with electrical resistivity surveys in cold continuous permafrost. *Geophysical Journal International*, *215*(2), 965–977. https://doi.org/10.1093/GJI/GGY321

Pimpirev, C., Stoykova, K., Ivanov, M., & Dimov, D. (2006). The sedimentary sequences of Hurd Peninsula, Livingston Island, South Shetland Islands: Part of the late Jurassic—Cretaceous depositional history of the Antarctic Peninsula. In D. K. Fütterer, D. Damaske, G. Kleinschmidt, H. Miller, & F. Tessensohn (Eds.), *Antarctica*. Springer. https://doi.org/10.1007/3-540-32934-X_30

Ramos, M., & Vieira, G. (2009). Ground surface Enthalpy balance based on borehole temperatures (Livingston Island, Maritime Antarctic). *The Cryosphere*, *3*(1), 133–145. https://doi.org/10.5194/tc-3-133-2009

Ramos, M., Vieira, G., Blanco, J. J., Gruber, S., Hauck, C., Hidalgo, M. A., & Tome, D. (2008). Active layer temperature monitoring in two boreholes in Livingston Island, Maritime Antarctic: First results for 2000–2006. In D. L. Kane & K. M. Hinkel (Eds.), *Ninth international conference on permafrost—Extended abstracts, June 29–July 3* (pp. 1463–1467). University of Alaska, Fair banks.

Ramos, M., Vieira, G., De Pablo, M. A., Molina, A., Abramov, A., & Goyanes, G. (2017). Recent shallowing of the thaw depth at crater lake, Deception Island, Antarctica (2006–2014). *Catena*, *149*, 519–528. https://doi.org/10.1016/j.catena.2016.07.019

Ramos, M., Vieira, G., de Pablo, M. A., Molina, A., & Jimenez, J. J. (2020). Transition from a subaerial to a subnival permafrost temperature regime following increased snow cover (Livingston Island, Maritime Antarctica). *Atmosphere*, *11*(12), 1332. https://doi.org/10.3390/atmos11121332

Ramos, M., Vieira, G., Gruber, S., Blanco, J. J., Hauck, C., Hidalgo, M. A., et al. (2008). *Permafrost and active layer monitoring in the Maritime Antarctic: Preliminary results from CALM sites on Livingston and deception islands*. U.S. Geological Survey and the National Academies. USGS OF-2007–1047, Short Research Paper 070. https://doi.org/10.3133/of2007-1047srp07

Scandroglio, R., Draebing, D., Offer, M., & Krautblatter, M. (2021). 4D quantification of alpine permafrost degradation in steep rock walls using a laboratory-calibrated electrical resistivity tomography approach. *Near Surface Geophysics*, *19*(2), 241–260. https://doi.org/10.1002/nsg.12149

Shiklomanov, N. I., Nelson, F. E., Streletskiy, D. A., Hinkel, K. M., & Brown, J. (2008). The circumpolar active layer monitoring (CALM) program: Data collection, management, and dissemination strategies. In *Proceedings of the 9th international conference on permafrost* (Vol. 1, pp. 1647–1652). Institute of Northern Engineering, University of Alaska.

Supper, R., Ottowitz, D., Jochum, B., Römer, A., Pfeiler, S., Kauer, S., et al. (2014). Geoelectrical monitoring of frozen ground and permafrost in alpine areas: Field studies and considerations towards an improved measuring technology. *Near Surface Geophysics*, *12*(1), 93–115. https://doi.org/10.3997/1873-0604.2013057

Tomaškovičová, S., & Ingeman-Nielsen, T. (2023). Quantification of freeze–thaw hysteresis of unfrozen water content and electrical resistivity from time lapse measurements in the active layer and permafrost. *Permafrost and Periglacial Processes*, *1*, 19. https://doi.org/10.1002/ppp.2201

Tso, C.-H. M., Kuras, O., Wilkinson, P. B., Uhlemann, S., Chambers, J. E., Meldrum, P. I., et al. (2017). Improved characterisation and modelling of measurement errors in electrical resistivity tomography (ERT) surveys. *Journal of Applied Geophysics*, *146*, 103–119. https://doi.org/10.1016/j.jappgeo.2017.09.009

Uhlemann, S., Dafflon, B., Peterson, J., Ulrich, C., Shirley, I., Michail, S., & Hubbard, S. S. (2021). Geophysical monitoring shows that spatial heterogeneity in thermohydrological dynamics reshapes a transitional permafrost system. *Geophysical Research Letters*, *48*(6), e2020GL091149. https://doi.org/10.1029/2020GL091149